Astron. Astrophys. 361, 601–613 (2000)

ASTRONOMY AND ASTROPHYSICS

Excitation of HCN in the circumstellar envelope of carbon stars. Maser emission and hyperfine line interaction

Dinh-V-Trung[1,2,3] **and Nguyen-Q-Rieu**[3]

[1] Institute of Astronomy and Astrophysics, Academia Sinica, P.O. Box 1–87, Nankang, Taipei 11529, Taiwan, ROC
[2] Institute of Physics, P.O. Box 429 BoHo 10000, Hanoi, Vietnam
[3] Observatoire de Paris, DEMIRM, 61 Avenue de l'Observatoire, 75014 Paris, France

Received 8 September 1998 / Accepted 9 June 2000

Abstract. We have investigated the excitation of the molecule HCN in the circumstellar envelopes of carbon stars, particularly the HCN(J=1-0) maser emission using a model which takes into account the collisional and radiative excitation, as well as the effect of the overlap of hyperfine lines.

We calculate consistently both the gas temperature and the mass loss rate based on the energy balance equation and the fitting of CO observations. In this way we can obtain more realistic data of the envelope.

In optically thin envelopes such as that around Y CVn, our results suggest that the HCN(J=1-0) transition is inverted by the absorption of 3 μm stellar photons which transfers the population to the (001) vibrational state and by subsequent cascades down to the fundamental state. Mutual amplification of hyperfine components results in HCN line profiles containing several strong maser spikes.

In thicker envelopes, such as IRC+10216, we find that HCN and $H^{13}CN$ are excited mainly by the absorption of infrared photons emitted by the warm dust at 14 μm. The HCN(J=1-0) and $H^{13}CN$(J=1-0) line profiles calculated by our model contain several features as observed. We also discuss the implication of our results on the mass loss history of IRC+10216.

Key words: masers – radiative transfer – stars: circumstellar matter – stars: individual: IRC+10216, Y CVn

1. Introduction

The expanding circumstellar envelopes around AGB stars have been studied extensively, especially in the millimeter and submillimeter regions. Strong CO and HCN emissions have been detected in the circumstellar envelope of carbon stars. Since CO molecule is very abundant in the envelope and is easily excited by collisions with H_2 molecules, observations of CO rotational lines have been used to determine several important parameters of the envelope such as the mass loss rate and the distribution of gas temperature. That task usually requires careful modelling of radiative transfer as well as the treatment of energy balance of the gas inside the envelope. Models of various degrees of sophistication have been constructed (Kwan & Hill 1977, Kwan & Linke 1982, Truong-Bach et al. 1991, Groenewegen 1994, Justtanont et al. 1994, Crosas & Menten 1997) to fit the CO observations. Ideally one would like to have observations of as many CO rotational lines as possible. However, observational data of the high-lying transitions of CO which are sensitive to dense and warm gas in the inner part of the envelope are scarce. Thus data from other molecular lines which probe the same inner region are particularly helpful in providing complementary observational constraints. In carbon stars HCN molecule is abundant, making it easy to detect. HCN also possesses a large permanent dipole moment (2.98 Debyes), as a result, its rotational transitions are more sensitive to high density gas in the envelope. Furthermore, radiative excitation by the absorption of infrared photons (Morris 1985) is expected to play an important role in exciting HCN molecules. Since its rotational levels are split into hyperfine levels the line overlap also contributes to redistribute the populations among hyperfine levels. Observationally, the overlap of hyperfine components also makes the observed HCN(J=1-0) profile from carbon stars larger than that of CO (Nguyen-Q-Rieu et al. 1987, Truong-Bach & Nguyen-Q-Rieu 1989). Thus, observations and a detailed modelling of HCN should provide further information on the physical conditions (gas density, temperature as well as the radiation field) in the inner regions of the envelope where HCN emissions arise.

Maser emissions in the HCN rotational transitions (J=1-0) and (J=2-1) in the excited vibrational states (02^00) and ($01^{1c}0$) have been observed in optically thick circumstellar envelopes (Guilloteau et al. 1987, Lucas & Cernicharo 1989). Interferometric observations of the HCN (02^00, J=1-0) transition in IRC+10216 (Lucas & Guilloteau 1992) together with narrow HCN (02^00, J=1-0) line seen in other carbon stars (Lucas et al. 1988) suggest that this maser is produced very close to the central star, probably in the region where the gas is still being accelerated.

The ground state HCN(J=1-0) and $H^{13}CN$(J=1-0) masers are first detected in the thin envelope of the carbon star Y CVn (Izumiura et al. 1987). Subsequent sensitive surveys of Olofsson et al. (1993b) and of Izumiura et al. (1995b) show that the ground state HCN(J=1-0) maser occurs in a number of other optically

Send offprint requests to: Dinh-V-Trung (trung@asiaa.sinica.edu.tw)

thin envelopes of carbon stars. The maser profiles usually contain strong spikes superimposed on broad features. However, the mechanisms responsible for the pumping of these masers still remain unexplained. The presence of maser emission in the HCN(J=1-0) transition makes the interpretation of observations and the determination of HCN abundance complicated (Olofsson et al. 1993b, Izumiura et al. 1995b).

There have been some efforts to study the excitation of HCN molecule in carbon stars, in particular the envelope of IRC+10216. Truong-Bach & Nguyen-Q-Rieu (1989) construct a LVG (large velocity gradient) model taking into account the infrared (IR) excitation and hyperfine line overlap in order to explain the interferometric observations of Bieging et al. (1984). Although their model can explain some major features of the HCN(J=1-0) line profile, a more realistic (non-local) model is needed to treat more appropriately the absorption of IR photons by HCN molecules and the overlap of hyperfine components. Dayal & Bieging (1995) made an improvement by calculating directly the absorption of IR photons by HCN molecules without relying on LVG approximation.

In this paper we investigate in detail the excitation mechanisms of HCN in the circumstellar envelopes of carbon stars using a non-local radiative transfer model including collisional and radiative excitation, as well as the overlap of hyperfine components.

The model is applied to two specific cases: the optically thin envelope of Y CVn and the optically thick envelope of IRC+10216. We propose that all HCN(J=1-0) hyperfine components in optically thin envelope of carbon stars such as Y CVn are inverted by the absorption of $3\,\mu$m stellar photons. High resolution observations of HCN(J=1-0) and $H^{13}CN$(J=1-0) towards the envelope of IRC+10216 are also modelled in order to determine the the abundance of HCN and $H^{13}CN$ in this envelope.

2. The model

2.1. Thermal balance model

In order to extract information on the mass loss rate and the gas temperature from CO observations, we have developed a model taking into account the heating and cooling of the gas in the circumstellar envelope. Our model is similar to that described earlier by Groenewegen (1994) and Crosas & Menten (1997). More details can be found in the appendix.

2.2. Description of the radiative transfer model

In our model we do not use the LVG approximation but integrate directly the equation of radiative transfer:

$$\frac{dI(\nu)}{ds} = -k(\nu)\, I(\nu) + \epsilon(\nu) \tag{1}$$

where k(ν) and $\epsilon(\nu)$ are the opacity and emissivity respectively at the frequency ν. For the transition between two energy levels i and j, the expressions of the opacity and the emissivity are:

$$k_{\rm ij}(\nu) \;=\; \frac{h\nu}{4\pi} B_{\rm ij} g_{\rm j} (n_{\rm j} - n_{\rm i}) \phi(\nu) \tag{2}$$

$$\epsilon_{\rm ij}(\nu) \;=\; \frac{h\nu}{4\pi} n_{\rm i} g_{\rm i} A_{\rm ij} \phi(\nu) \tag{3}$$

where A_{ij} and B_{ij} are the Einstein coefficients, g_i are the statistical weights and $\phi(\nu)$ is the line profile determined by local microturbulence and thermal motion; n_i and n_j are the populations per magnetic sublevel. The line source function for this transition is:

$$S_{\rm ij} = \frac{2h\nu^3}{c^2} \frac{n_{\rm i}}{n_{\rm j} - n_{\rm i}} \tag{4}$$

In the presence of dust particles and line overlap, we use:

$$k(\nu) \;=\; \sum_{\rm i \succ j} k_{\rm ij}(\nu) + k_{\rm c}(\nu) \tag{5}$$

$$\epsilon(\nu) \;=\; \sum_{\rm i \succ j} \epsilon_{\rm ij}(\nu) + \epsilon_{\rm c}(\nu) \tag{6}$$

where k_c and ϵ_c are the opacity and emissivity of the dust. The index runs through all lines which contribute to the opacity and to the emissivity at frequency ν.

$$k_{\rm c} \;=\; \pi a^2 Q_\nu n_{\rm d} \tag{7}$$

$$\epsilon_{\rm c} \;=\; \pi a^2 Q_\nu n_{\rm d} B_\nu(T_{\rm d}) \tag{8}$$

where a, n_d and Q_ν are the grain radius, the dust density and the absorption efficiency, respectively. $B_\nu(T_d)$ is the Planck function at the dust temperature T_d. The source function in the presence of line overlap and dust continuum emission is:

$$S(\nu) = \epsilon(\nu)/k(\nu) \tag{9}$$

The mean intensity J_{ij} which appears in the statistical equilibrium equations is:

$$J_{\rm ij} = \frac{1}{4\pi} \int d\Omega \int d\nu \phi_{\rm ij}(\nu) I(\nu) \tag{10}$$

The system of the statistical equilibrium equations coupled with the radiative transfer equations is solved by iterative method. One drawback of this Λ-scheme is its very low convergence rate. One simple way to overcome this difficulty when the typical optical depths are not too large is to use the acceleration technique proposed by Auer (1987, 1991). Auer demonstrated that the technique can increase substantially the rate of convergence. The effectiveness of this method is verified in our calculations. The convergence is achieved when the change of the populations between two successive iterations is less than 10^{-3}.

2.3. Molecular data of HCN and CO

HCN is a linear molecule and its energy diagram is presented in Fig. 1. There are three possible vibrational modes: two stretching modes ν_1, ν_3 and one degenerate bending mode ν_2. Due to l-type doubling, the (010) bending-mode is split into ($01^{1c}0$) and ($01^{1d}0$) levels. Similarly, the (020) vibrational level is split into

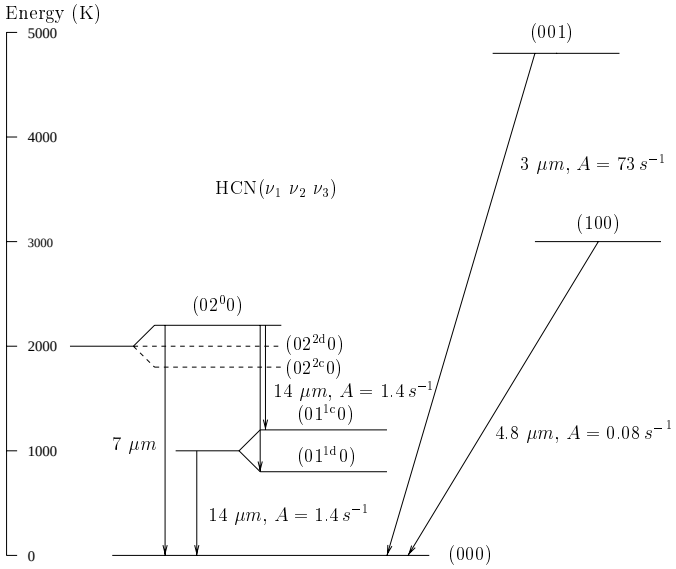

Fig. 1. Energy levels of HCN considered in the model. Dotted lines stand for levels which do not connect with the ground state. The l-type doubling is shown not to scale.

Table 1. Parameters used in our standard model for Y CVn.

$T_{effective}$	2730 K *
Luminosity	4.9 10^3 $L_\odot$
R_*	2.2 10^{13} cm
Distance	218 pc
V_{exp}	8 km s^{-1}
r_0	7.5 10^{13} cm
R_{min}	10^{14} cm
R_{max}(CO)	4 10^{16} cm
R_{max}(HCN)	2 10^{15} cm
[CO] / [H_2]	6.6 10^{-4}
[HCN] / [H_2]	5.5 10^{-5}
$^{12}C/^{13}C$	3.5
$\dot{M}$	1.5 10^{-7} $M_\odot$/yr
δ	1.8 10^{-3} +
a_d	0.05 μm
ρ_d	1.85 g
$\tau_{1\mu m}$	0.05
$\kappa_{60\mu m}$	80 cm^{2}g^{-1}
V_{turb}	0.5 kms^{-1}

* from Izumiura et al. (1995b)
+ derived from dust opacity at 1 μm using formula (12)

(02^{0}0), (02^{2c}0) and (02^{2d}0) respectively. Selection rules allow only the level (02^{0}0) to be connected with the ground state. The (001) and (100) states correspond to two stretching modes. Each rotational level designated by quantum number J of HCN is further split into three hyperfine levels **F= J+I**, where I=1 is the spin of the nitrogen nucleus. For low lying rotational levels the energy separation between hyperfine levels is so large that the corresponding hyperfine lines are not completely blended. We use the data from GEISA database to determine the frequencies and transition probabilities for vibration-rotation transitions of HCN. Frequency shifts between hyperfine components of the first three rotational transitions are taken from Maki (1974). Hyperfine lines within other rotational and vibration-rotation transitions are considered to be completely blended.

Collisional rates between hyperfine levels are calculated from the rates between rotational levels (Green & Thaddeus 1974) using the procedure proposed by Neufeld & Green (1994).

For CO molecule, we use an IR dipole moment of 0.11 Debye determined by Goorvitch & Chackerian (1994). Collisional rates between CO and H_2 molecules are taken from Flower & Launay (1985). As we need the collisional rates at all temperatures and for all rotational levels considered, we use the formulae given by De Jong et al. (1975) to extrapolate the necessary collisional rates.

3. Optically thin envelope: Y CVn

In this section we discuss the excitation of HCN molecule in the optically thin envelopes of bright carbon stars. We choose to model the envelope of Y CVn. The distance to this star is known to be 218 $\pm$ 30 pc from Hipparcos data. The dust envelope of Y CVn is known to be optically thin (Lorenz-Martin & Lefèvre 1994). The near infrared emission comes mainly from the central star with an effective temperature of 2730 K (Izumiura et al. 1995b) and plays an important role in exciting HCN molecules. Furthermore, observations of several CO transitions towards Y CVn are available making possible the determination of the mass loss rate and the temperature structure inside the envelope. We first fit the CO data using the energy balance model and then apply our non-local radiative transfer model to investigate the excitation of HCN molecule, especially the pumping of (J=1-0) maser.

3.1. CO lines

In our energy balance model we include the radiative cooling due to ^{12}CO, ^{13}CO as well as HCN and H^{13}CN. As Y CVn is a J-star with an abundance ratio $^{12}C/^{13}C \sim 3.5$ (Lambert et al. 1986), the contribution of ^{13}CO to the cooling term is substantial. The cooling due to HCN is limited to the inner region of the envelope where HCN is present. Thus the gas temperature in the outer part of the envelope and the predictions of CO lines intensity are not much affected by the choice of HCN abundance. It turns out that the contribution of HCN molecule to the total cooling term is about 20%. In our standard model for Y CVn only the gas mass loss rate is the free parameter to be determined. Other parameters are taken from the literature. We use a constant CO abundance of 6.6 10^{-4} which is estimated by Olofsson et al. (1993b) using static LTE model stellar atmospheres. The outer radius of the CO envelope is estimated to be 4 10^{16} cm based on interferometric observations by Neri et al. (1998). The abundance of HCN is simply adjusted around the estimate of Olofsson et al. (1993b).

In the outer part of the envelope where CO emission originates, the expansion velocity is nearly constant. But in the inner part where HCN molecule exists, the gas velocity may vary

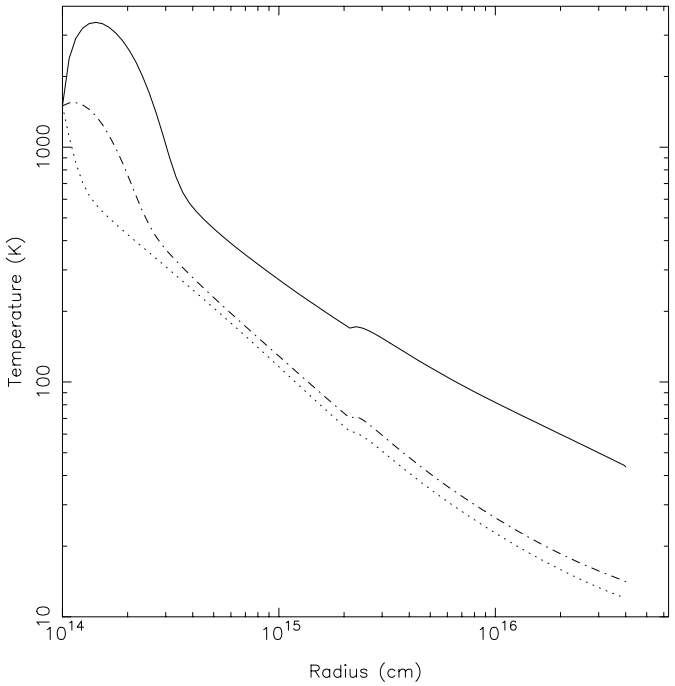

Fig. 2. Gas temperature as a function of radius. The solid line represents the gas temperature from our standard model ($\dot{M}$=1.5 10^{-7}M$_\odot$/yr, $\tau_{1\,\mu m}$=0.05). The dotted line is from our model-I ($\dot{M}$=1.5 10^{-7}M$_\odot$/yr, $\tau_{1\,\mu m}$=0.01) and the dash-dotted line is from our model-II ($\dot{M}$=3 10^{-7}M$_\odot$/yr, $\tau_{1\,\mu m}$=0.05)

significantly. We adopt the following law (Deguchi & Nguyen-Q-Rieu 1990) for the gas velocity:

$$v(r) = V_{\rm exp}(1 - \frac{r_0}{r})^{0.5} \tag{11}$$

where r_0 is chosen so that the velocity of the gas at the inner radius is half of the expansion velocity. The expansion velocity $V_{\rm exp}$ of Y CVn is determined by Olofsson et al. (1993b) and Knapp et al. (1998) from CO observations to be 8 kms^{-1}. Besides the thermal linewidth we include a turbulence velocity of 0.5 kms^{-1} (FWHM $\sim$ 0.83 kms^{-1}) which represents a possible turbulence in the envelope. Observations of CO(J=1-0), CO(J=2-1) (Groenewegen et al. 1996) and CO(J=3-2) (Knapp et al. 1998) rotational lines are used to estimate the mass loss rate and the distribution of gas temperature. One important parameter which controls the heating process inside the envelope is the dust optical depth. This quantity is related to other parameters as follows:

$$\begin{aligned}\tau_\lambda &= \pi a_{\rm d}^2\, Q_\lambda \int_{\rm r_c}^{\infty} n_{\rm d}(r)\, dr \\ &= \frac{3\,\delta\,\dot{M}}{16\pi\, r_c\, \rho_{\rm d}\, v_{\rm d}} \cdot \left(\frac{Q_\lambda}{a_{\rm d}}\right)\end{aligned} \tag{12}$$

where $a_{\rm d}$ is the radius of the dust particle, $\rho_{\rm d}$ is the grain specific density, v_d is the dust velocity, δ is the dust to gas ratio, r_c is the inner radius of the envelope (r_c = R$_{\rm min}$). The quantity Q_λ is the dust absorption coefficient at the wavelength λ. This quantity is related to the usual dust opacity κ_λ by the formula $\kappa_\lambda = (3Q_\lambda/4a_d\rho_d)$. We assume that the dust is composed entirely of amorphous carbon with an opacity at 60 μm of about 80 cm^2g^{-1} (Rouleau & Martin 1991). For amorphous carbon dust particle with size much less than the wavelength, it was shown that the ratio ($Q_\lambda/a_{\rm d}$) varies with wavelength as λ^{-1}. This law is then used to calculate the average absorption coefficient (or the momentum transfer efficiency) of the dust which is needed to estimate the heating rate due to dust-gas collisions.

$$Q/a_{\rm d} = \frac{\int_0^\infty F_\lambda\, Q_\lambda/a_{\rm d}\, d\lambda}{\int_0^\infty F_\lambda\, d\lambda} \tag{13}$$

where F_λ is the spectral energy distribution in the envelope. If the dust envelope is optically thin, the function F_λ is essentially the spectral energy distribution of the central star. In the case of Y CVn, Lorenz-Martin & Lefèvre (1994) derived an optical depth of 0.05 for the dust envelope at 1 μm and the size of dust particles about 0.05 μm. We thus estimate the momentum transfer efficiency Q to be 0.04.

Our standard model can fit reasonably the CO line intensity with a mass loss rate of $\dot{M}\sim$1.5 10^{-7} M$_\odot$/yr which is comparable to the values 1.2 10^{-7} M$_\odot$/yr derived by Olofsson et al. (1993a) and 1.1 10^{-7} M$_\odot$/yr from Knapp et al. (1998) who used a semi-empirical relation (Knapp & Morris 1985) which is more appropriate to a statistical study. The corresponding gas temperature distribution is presented in Fig. 2. The CO(J=2-1) peak intensity is slightly overestimated. We find that it's very difficult to make a good fit to the line shape of CO(J=1-0) and CO(J=2-1) transitions in the standard model. The predicted CO(J=3-2) line is also larger and less rounded than the observed one. As the parameters for the dust envelope are all fixed in the standard model, for a mass loss rate of 1.5 10^{-7} M$_\odot$/yr the heating is quite high which results in a high gas temperature in the envelope. In this case the shape of the calculated CO(J=1-0) and CO(J=2-1) profiles is slightly double-peaked. If the heating rate is reduced (by lowering the dust opacity $\tau_{1\mu m}$) or we increase the cooling rate by increasing the mass loss rate, the gas temperature will be reduced and the line shape will become parabolic as observed. We check the above expectations by calculating other models: in model-I we keep the same mass loss rate at 1.5 10^{-7} M$_\odot$/yr and lower the dust optical depth to $\tau_{1\,\mu m}$ = 0.01; in model-II we increase the mass loss rate to 3 10^{-7} M$_\odot$/yr. It's evident from Fig. 2 that with little heating the gas temperature in model-I drops very quickly with distance to about 10 K at the outermost part of the envelope. Since the number density of dust particles in model-II is the same as in the standard model the heating term actually decreases (Eq. A1) while the cooling term increases with higher mass loss rate. Thus the gas temperature is lower than in the standard model. The calculated CO line profiles from these models are given in Fig. 3.

CO(J=1-0) and CO(J=2-1) lines from model-I are in good agreement with observations while predicting a lower intensity for the CO(J=3-2) line. Smaller dust content changes significantly the heating in the envelope and results in lower gas temperature. The optical depths of CO(J=1-0) and CO(J=2-1) lines are now higher than in the standard model because less CO molecules are excited to higher rotational levels. The line

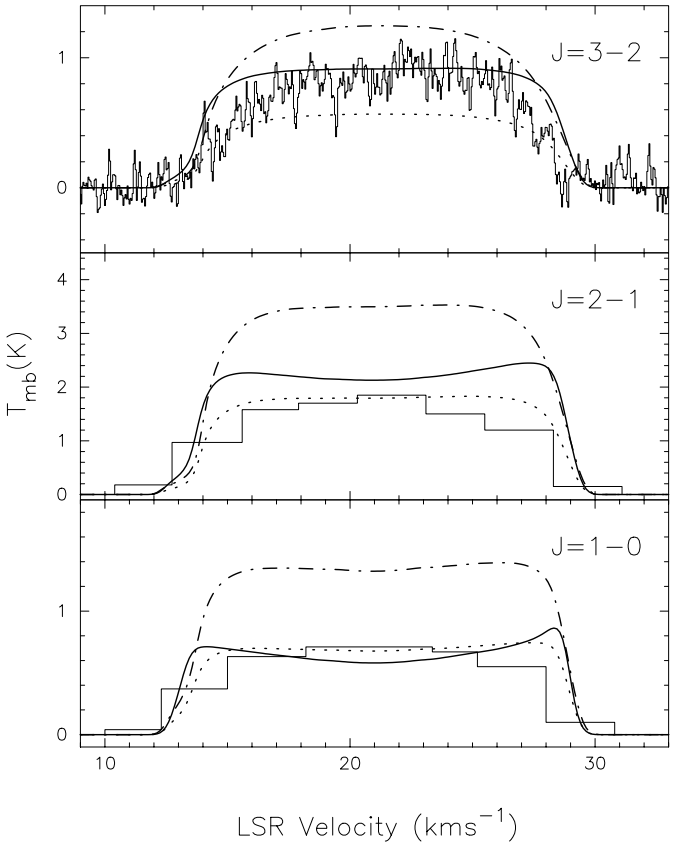

Fig. 3. Observed and calculated CO spectra for Y CVn. The histograms represent CO observations. The thick solid lines represent CO profiles from our standard model. The dotted lines represent CO profiles from our model-I. The dash-dotted lines represent the predictions of model-II. The CO observations are taken from Groenewegen et al. 1996 and Knapp et al. 1998

profiles have parabolic shape. Our model-II, which has higher mass loss rate, overestimates the intensity of CO(J=3-2) line but its line shape is in better agreement with observation of Knapp et al. (1998). On the other hand, the model-II predicts much higher intensity for other CO lines.

One conclusion drawn from our results is that in order to achieve a good agreement with observations the mass loss rate as well as the dust to gas ratio in Y CVn can not be constant with time. In the outer part of the envelope there is less dust and the mass loss rate is lower (model-I). The dust content and/or the gas mass loss rate increase with time to the present values. It seems probable that the current mass loss rate can be as high as 3 10^{-7} $M_\odot$/yr since the model-II produces CO(J=3-2) line shape in better agreement with observations.

3.2. HCN(J=1-0) maser emission from Y CVn

We assume that in the envelope of Y CVn the IR photons come mainly from the central star. This assumption is justified since the dust envelope of Y CVn is optically thin, $\tau_{1\mu m}$ = 0.05 (Lorenz-Martin & Lefèvre 1994). We estimate that the dust envelope contributes roughly 20% to the flux at 14 μm and about 10% at 7 μm. At 3 μm the contribution of the warm dust is insignificant. Therefore we can neglect the role of the dust envelope in the case of Y CVn.

The size of the HCN envelope is determined from the photodissociation process of HCN molecules by the interstellar UV photons. Recent high resolution observations of HCN(J=1-0) line (Lindqvist et al. 1995) suggest that the real size of the HCN envelope is usually larger than predicted by photodissociation models (Olofsson et al. 1993b). For Y CVn, we use a cutoff radius of 2 10^{15} cm, which is slightly larger than the value of 1.2 10^{15} cm given in Olofsson et al. (1993b).

As the number of levels becomes prohibitively large when hyperfine splitting of rotational levels is taken into account, it's necessary to consider only vibrational states whose vibration-rotation transitions play important role in the excitation of HCN. We will show in the next section that the transitions (001) $\rightarrow$ (000) at 3 μm is the most important with a small contribution from the transitions ($01^{1c}0$) $\rightarrow$ (000). Thus, we retain in our model only the ground state, the ($01^{1c}0$) and ν_3 = 1 vibrational states. All rotational levels up to J_{max}=12 are included. We find that both the standard model and model-I predict too small intensity for the HCN(J=1-0) line within the reasonable range of HCN abundance. The HCN abundance of 5.5 10^{-5} used in our model is higher than the value given by Olofsson et al. (1993b). Although the inversion of the HCN(J=1-0) transition occurs in both models, the optical depths in the radial direction are small ($\sim$ -5). A low mass loss rate (1.5 10^{-7} $M_\odot$/yr) in these models reduces the number of available HCN molecules in the masing region and consequently the optical depth is lower. In contrary, model-II which corresponds to a mass loss rate of 3 10^{-7} $M_\odot$/yr predicts the intensity of the HCN(J=1-0) line in agreement with observations. The calculated HCN(J=1-0) profile from Y CVn including hyperfine splitting is shown in Fig. 4. Our calculations also show that the calculated HCN(J=1-0) profile contains several strong maser spikes. These features occur as a result of maser and mutual amplification of F=1-1 and F=2-1 hyperfine components. Since the optical depth is proportional to the statistical weight of the upper level of hyperfine transitions (3 and 5 for F=1-1 and F=2-1 transitions, respectively), these components have highest negative optical depths in comparison with the F=0-1 transition. We find that the largest optical depth in the radial direction in model-II is about -7. The F=1-1 component tends to be inverted over almost the entire HCN envelope while the inversion of the F=0-1 component is confined to the inner region of the envelope (Fig. 5). Therefore the intensity of the F=0-1 hyperfine component is in general very weak (Fig. 4). It should be noted that the HCN(J=1-0) maser intensity is relatively insensitive to the change of the gas temperature in the envelope when the mass loss rate is low. In our standard model and model-I the calculated intensities are very similar although the gas temperature changes by nearly a factor of 2. That can be attributed to the weak dependence of collisional rates of HCN at high temperature (a few hundreds K) and the dominant role of radiative excitation in the inversion of J=1-0 transition.

The peak antenna temperature predicted for the 45m telescope with a 21 arcsec beam is about 4 K, in agreement with

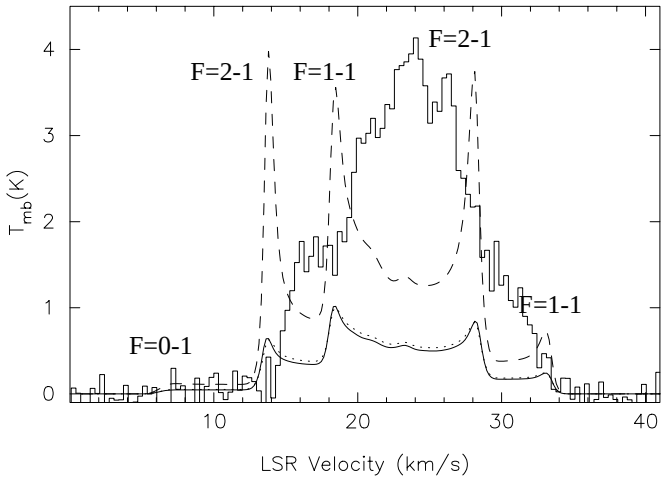

Fig. 4. The calculated HCN(J=1-0) profiles from Y CVn for the 45m telescope with a 21 arcsec beam. The standard model, model-I and model-II are represented by solid line, dotted line and dashed line, respectively. The histogram corresponds to the HCN(J=1-0) line observed with the BIMA array and convolved to 21 arcsec resolution.

single dish observations of Izumiura et al. (1995b). In Fig. 4 we also compare our result with the BIMA-array observations of HCN(J=1-0), kindly provided to us by Dr. R. Forster. The envelope of Y CVn seems to be not resolved with a synthesized beam of 3.9×2.6 arcsec. We convert the HCN(J=1-0) spectrum into the main beam temperature unit of the 45m telescope to facilitate the comparison with previous observations (Izumiura et al. 1995b) and with our results. The HCN(J=1-0) spectrum is nearly the same as that obtained with the 45-m telescope by Izumiura et al. (1995b). It can be seen from Fig. 4 that the velocity of maser peaks calculated by our model does not correspond exactly to the observed ones. But a closer look indicates that the peaks in the observed profile seems to fit into the regular pattern of hyperfine transitions. The features at $V_{\rm LSR}\sim15\,{\rm kms}^{-1}$ and $26\,{\rm kms}^{-1}$ are probably the blue-shifted and red-shifted components of F=2-1 transition. The other features near $V_{\rm LSR}\sim21\,{\rm kms}^{-1}$ and $30\,{\rm kms}^{-1}$ may also belong to the F=1-1 transition. These peaks are displaced in velocity with respect to the calculated ones. Therefore it is possible that the gas velocity in the inner part of the envelope is not as high as expected from our adopted velocity law (Eq. 11). We now use the same mass loss rate and temperature distribution as in model-II but lower the terminal velocity $V_{\rm exp}$ to $6\,{\rm kms}^{-1}$. To produce the same intensity as observed the abundance of HCN is found to be $4\ 10^{-5}$. Thus the number density of HCN molecules in the envelope is about the same in both model-II and this case. The result of our calculations is presented in Fig. 6. The position in velocity of maser features is now in relatively good agreement with observations. Only the peak near the central velocity ($V_{\rm LSR}\sim26\,{\rm kms}^{-1}$) remains difficult to explain. This fact suggests that the real distribution of matter in the HCN envelope may not be spherical and/or the velocity field is more complicated than assumed in our model.

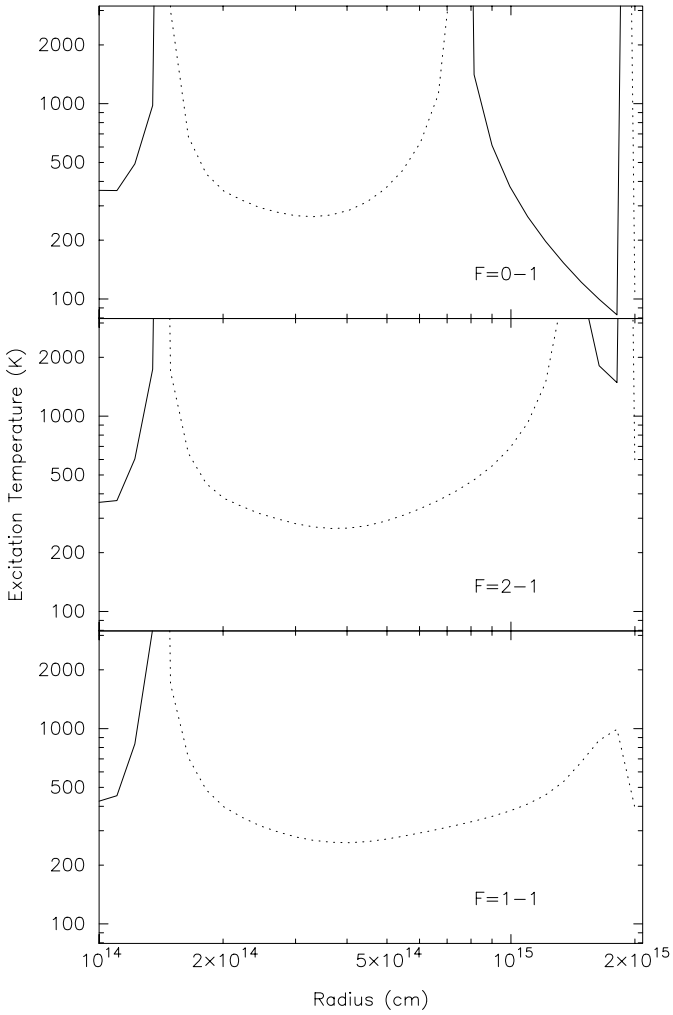

Fig. 5. Excitation temperature T_{ex} of J=1-0 hyperfine components calculated in model-II. Negative values of T_{ex} are represented by dotted lines.

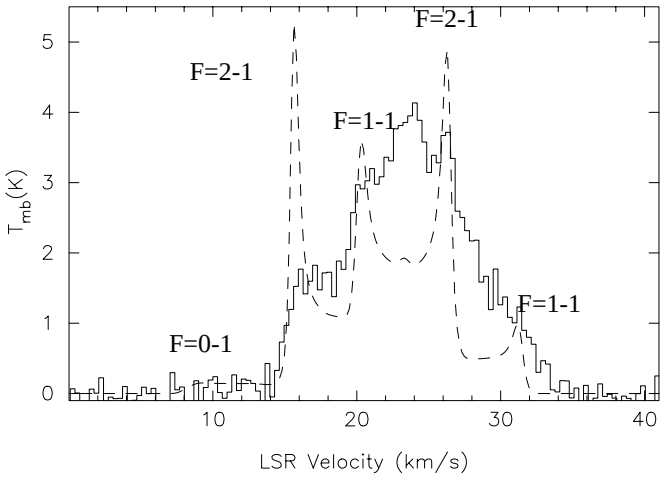

Fig. 6. The calculated HCN(J=1-0) profile (dashed line) for Y CVn. The histogram corresponds to the HCN(J=1-0) profile observed with the BIMA array and convolved to 21 arcsec resolution. Parameters of model-II are used here, except the expansion velocity is assumed to be $6\,{\rm kms}^{-1}$.

More interestingly, the HCN(J=1-0) maser emission from other bright carbon stars, such as W Ori, occasionally shows clearly the triple-peaked profile (Olofsson et al. 1998), similar to that calculated from our models (Fig. 4).

As the HCN(J=1-0) maser is pumped by stellar IR photons, its intensity varies during a stellar cycle. In addition, HCN(J=1-0) is a non-saturated maser. Therefore its intensity can vary strongly with the change of local physical conditions. The variability of the HCN maser is observed in Y CVn and in some other carbon stars (Olofsson et al. 1993b, 1998; Izumiura et al. 1995b). According to our results the strongest inversion appears at radii of a few 10^{14} cm. This region is very close to the central star and the dust forming locations. As a result, cyclic variation of the luminosity of the central star, stellar pulsation, dust formation etc... can create violent dynamical events such as shock waves, local density enhancement of gas density on a timescale comparable to the stellar cycle. Thus the variability of HCN(J=1-0) maser is not unexpected. In some aspects HCN(J=1-0) maser is similar to SiO masers in O-rich circumstellar envelopes although the intensity is an order of magnitude weaker.

3.3. HCN(J=1-0) maser emission and its dependence on mass loss rate

In this section we study how the pumping of HCN(J=1-0) line in optically thin envelope of carbon stars is influenced by other processes such as collisions, the absorption of stellar photons by different vibration-rotation transitions of HCN. We use the same parameters considered in model-II of the Y CVn envelope. For simplicity, we consider all rotational levels up to J_{max} = 12 in each vibrational state presented in Fig. 1. Since the effect of hyperfine splitting on the line profile is discussed in previous section, we neglect hyperfine splitting here. As in previous section, we also assume that IR photons come mainly from the central star.

Our model shows that in the envelope of optically thin envelope of carbon stars like Y CVn, HCN molecules are radiatively excited by the absorption of the 3 μm stellar photons. At a radius of 3 10^{14} cm the relative rates at which HCN molecules being transfered out of ground state J = 1 rotational level due to R-branch transitions to (001), ($01^{1c}0$) and ($02^{0}0$) are 42:9:1, respectively. The ($01^{1d}0$) vibrational level is connected to the ground state only through the Q branch transitions (Δ J = 0). An absorption of a 14 μm photon is followed immediately by radiative decay to the initial rotational level in the ground state. Therefore, the absorption in the Q branch to the ($01^{1d}0$) level contributes insignificantly to the excitation of rotational levels in the ground state of HCN molecule. Clearly the near infrared radiation from the central star at 3 μm plays a dominant role in the excitation process. Radiative excitation tends to create non-LTE populations in the rotational levels of HCN molecule. This interesting effect of the radiation field was pointed out earlier by Schönberg (1988). The non-LTE effect is strongest in the J=1-0 transition. In our model, the J=1-0 transition is found to be inverted over a large part of the envelope. The expansion velocity of the gas according to our adopted law (Eq. 11) has small velocity gradient in the region where HCN(J=1-0) line is strongly inverted. In this case, maser emission is amplified preferentially in the radial direction and gives rise to a double-peaked profile (Fig. 7). The intensity of HCN(J=1-0) emission is almost 4 times higher than for CO(J=1-0) line. As a result, it would be impossible to explain the strength of HCN(J=1-0) emission in terms of thermal emission, unless we adopt very high gas temperature and unrealistically large HCN abundance.

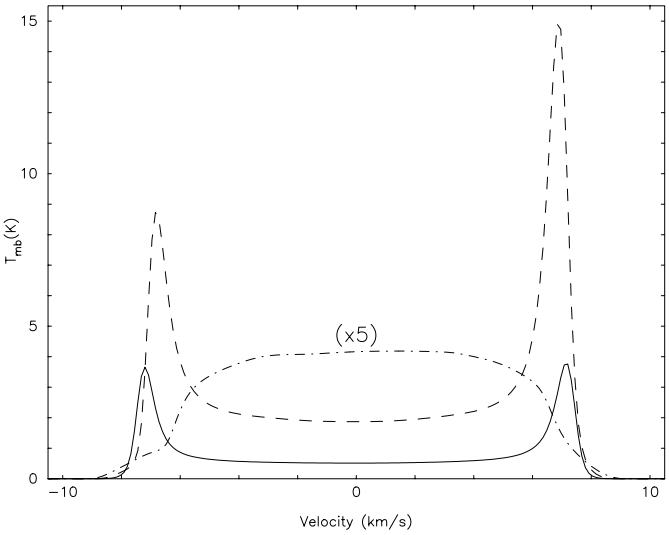

Fig. 7. Calculated HCN(J=1-0) profiles from envelopes with different mass loss rates. The angular resolution is 21 arcsec, appropriate for the 45m telescope. The solid line represents the model with $\dot{M}$ = 3 10^{-7} $M_\odot$/yr. The dashed line represents the model with $\dot{M}$ = 10^{-6} $M_\odot$/yr. The dashed-dotted line is the HCN(J=1-0) profile (multiplied by 5) calculated for $\dot{M}$ = 2 10^{-6} $M_\odot$/yr. Hyperfine structure of rotational levels is not considered.

Based on the observations of a sample of AGB stars, Olofsson et al. (1998) noted that the HCN(J=1-0) maser appears preferentially in optically thin envelope of bright carbon stars. In addition, there seems to be a steep decrease of the HCN(J=1-0) line intensity for carbon stars with higher mass loss rates. The trend suggests that as the gas density increases with mass loss rate, collisional excitation becomes stronger and thermalizes the HCN(J=1-0) transition. We have investigated this possibility by running our model with different mass loss rates while keeping other parameters unchanged. Our model shows that the HCN(J=1-0) maser is quenched at a mass loss rate around 2 10^{-6} $M_\odot$/yr due to collisions (Fig. 7). The HCN(J=1-0) line shape becomes parabolic as in the case of thermally excited lines from circumstellar envelopes. Furthermore, the 3 μm stellar radiation needed to create the inversion of the HCN(J=1-0) transition is also attenuated by HCN molecules near the inner radius of the envelope.

4. Optically thick envelope: IRC+10216

The thick envelope of IRC+10216 is the best studied circumstellar envelope thanks to its small distance ($\sim$150 pc) and its

high luminosity in the infrared and radio regions. Many high quality observations of CO rotational lines are available. The bunk of data make IRC+10216 an ideal object to test the models of radiative transfer and excitation of CO molecule. Several authors (Kwan & Linke 1982, Nguyen-Q-Rieu et al. 1984, Truong-Bach et al. 1991, Crosas & Menten 1997, Skinner et al. 1999) have developed radiative transfer models based on different techniques to fit CO observations. Furthermore, the dust envelope of IRC+10216 is also extensively investigated (Le Bertre 1987, Martin & Rogers 1987, Ridgway & Keady 1988, Winters et al. 1994, Danchi et al. 1994, Groenewegen 1997). We now know that the mass loss rate from IRC+10216 is a few 10^{-5} $M_\odot$/yr. The dust envelope and most of CO lines are optically thick. Stellar photons are therefore reprocessed by the dust envelope and re-emitted at longer wavelengths. The excitation of HCN molecule will be totally different from the case of optically thin envelope, such as Y CVn. In the envelope of IRC+10216 we expect an interplay between radiative excitation by IR photons from the warm dust, collisional excitation and the overlap of hyperfine lines.

To study these processes we first derive the mass loss rate and the gas temperature in IRC+10216 by fitting the CO observations. We then apply our radiative transfer model to HCN and its isotope $H^{13}CN$ using high angular resolution observations of Dayal & Bieging (1995) as the principal constraint to the model.

4.1. CO rotational lines

For IRC+10216, we have the most reliable observations of a number of CO rotational lines. Recently, Crosas & Menten (1997) used the Monte-Carlo method to solve the radiative transfer of CO and ^{13}CO in IRC+10216. The results of their model favor a constant mass loss rate of 3.25 10^{-5} $M_\odot$/yr. They also found that CO molecules are mostly excited by collision since IR photons at 4.6 μm are heavily absorbed in the inner region of the envelope due to the high optical depth of vibration-rotation transitions. We adopt here the parameters derived by Crosas & Menten (1997) except for the choice of the turbulence velocity $V_{\rm turb}$ in the envelope. For CO lines, the shape of the emergent profiles has a weak dependence on this parameter. On the other hand, the value of turbulence velocity affects significantly the HCN(J=1-0) and $H^{13}CN$(J=1-0) line profiles as discussed more thoroughly in the next section. We set $V_{\rm turb}$ equal to 0.5 kms^{-1} for which the model gives a good fit to the HCN(J=1-0) line profile. In our model we include all rotational levels in the fundamental vibrational state up to J=20 for CO and J=25 for HCN. All the parameters we use for IRC+10216 are given in Table 2. The improvement over the model of Crosas & Menten (1997) is the inclusion in the cooling term of the contribution of HCN molecule and its isotope $H^{13}CN$. As a result, we find that it is necessary to increase the momentum transfer coefficient of dust particles to Q = 0.03 (for $r < 10^{16}$ cm) and Q = 0.02 (for $r > 10^{16}$ cm) in order to maintain approximately the same temperature distribution and a good fit to CO observations. The increase in Q raises the heating due to dust-gas collision and compensates for the cooling due to HCN and $H^{13}CN$.

Table 2. The adopted and calculated parameters for IRC+10216.

Distance	150 pc
Luminosity	1.18 10^4 $L_\odot$
$\dot{M}$	3.25 10^{-5} $M_\odot$/yr
$V_{\rm exp}$	14 kms^{-1}
r_0	3.6 10^{14} cm
$R_{\rm min}$	10^{15} cm
$R_{\rm max}$(CO)	3 10^{17} cm
$R_{\rm max}$(HCN)	6 10^{16} cm
$[CO]/[H_2]$	6.0 10^{-4}
$[H^{13}CN]/[H_2]$	4.5 10^{-7}
$[HCN]/[H_2]$	2.5 10^{-5}
a_d	0.05 μm
ρ_d	1.85 g
δ	0.01
Q	0.03 for $r < 10^{16}$ cm
	0.02 for $r > 10^{16}$ cm
$V_{\rm turb}$	0.5 kms^{-1}

The calculated gas temperature distribution is very similar to that obtained by Crosas & Menten (1997) (Fig. 8). In the inner region of the envelope we find that HCN and $H^{13}CN$ contribute about 30% to the total cooling rate. Closer to the central star HCN cooling is known to dominate over CO cooling (Cernicharo et al. 1996). This region is expected to be quite small ($r < 10^{15}$ cm and has high kinetic temperature ($\sim$ 1200 K). The influence of such small region on the temperature distribution is expected to be minimal as we are more interested on the large scale structure in the envelope. It should be noted that the model of Crosas & Menten (1997) and ours use different approaches and different values of the turbulence velocity to calculate the cooling term. The two models produce nearly identical results. Probably for IRC+10216 the exact value of the turbulence velocity and the method to solve the radiative transfer problem (non-local or LVG) are not important to the calculation of population in each energy level of the molecule. Instead, they may have strong influence on the predicted line intensities (HCN rotational lines for example).

The calculated CO profiles are presented in Fig. 9. Our results match satisfactorily the CO observations.

4.2. Thermal emissions of $H^{13}CN$(J=1-0) and HCN(J=1-0)

The HCN(J=1-0) and $H^{13}CN$(J=1-0) transitions are observed towards the envelope of IRC+10216 by Dayal & Bieging (1995) using the BIMA array. Both emission lines are thermal and thanks to high angular resolution (8 arcsec) achieved with the BIMA array, hyperfine structure is clearly present in the observed spectra toward the center position of IRC+10216 (Fig. 10 and Fig. 13). The interferometric maps also show an extended emitting region with circular symmetry. In order to interpret these observations, Dayal & Bieging (1995) used a radiative transfer model for $H^{13}CN$ which includes collisional excitation

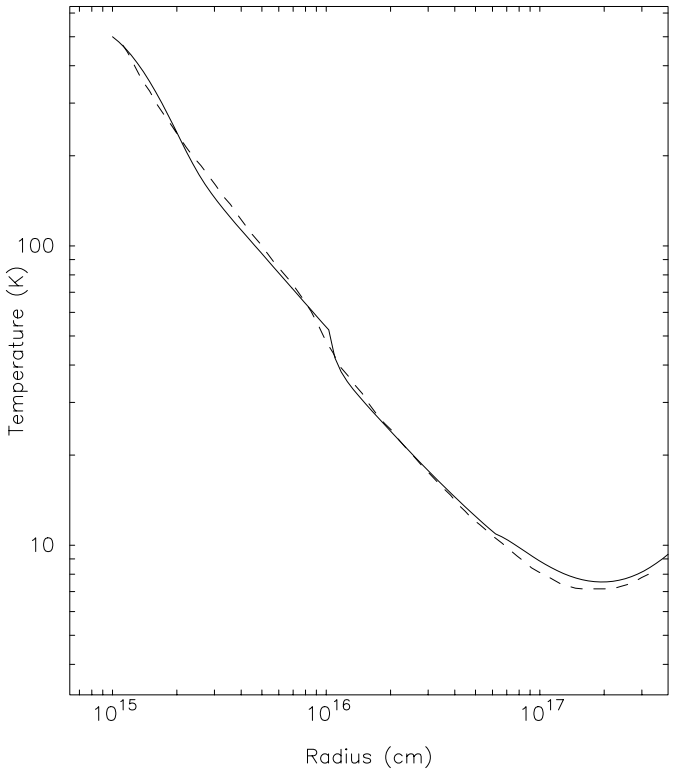

Fig. 8. Gas temperature distribution in IRC+10216. The dashed line represents the gas temperature derived by Crosas & Menten (1997). The solid line is the temperature calculated with our energy balance model.

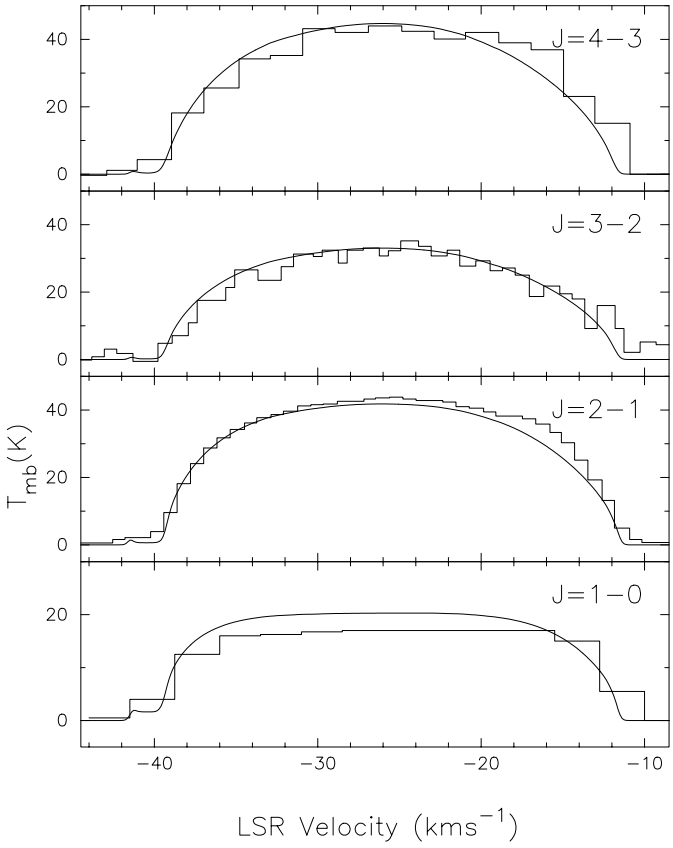

Fig. 9. IRC+10216. Comparison between model results (solid line) with observed CO line profiles (histogram) taken from Crosas & Menten (1997). The telescope beams for CO(J=1-0), CO(2-1), CO(3-2) and CO(4-3) lines are 21 arcsec, 12 arcsec, 20 arcsec and 11 arcsec respectively.

and infrared absorption at 14 μm. However, their model does not treat the overlap between hyperfine transitions. Instead, Dayal & Bieging (1995) estimate the population of a hyperfine level by multiplying the population of the corresponding rotational level by an arbitrary factor which is determined subsequently by fitting the observed $H^{13}CN$(J=1-0) data. As a result, their method represents only an approximate treatment of the interaction between hyperfine components of $H^{13}CN$(J=1-0) line.

In our model, the continuous distribution of the warm dust in the envelope of IRC+10216 is considered explicitly using the parameters determined by Le Bertre (1987). Since the dust envelope of IRC+10216 is optically thick in the optical and near infrared regions, stellar photons are absorbed by the warm dust and re-emitted at longer wavelengths. Only the IR emission at 14 μm from the warm dust is strong enough to excite the HCN and $H^{13}CN$ molecules. Therefore we include in our model only the (000), ($01^{1c}0$) vibrational states. We also take into account the variation of the $H^{13}CN$ and HCN abundances as a function of radius due to the effect of photodissociation by the external UV field, using the same parameters as Truong-Bach & Nguyen-Q-Rieu (1989). The HCN and $H^{13}CN$ abundances are found to remain nearly constant in the envelope except in the outermost layer.

For $H^{13}CN$ molecule, the best fit from our model is presented in Fig. 10 with an abundance of $4.5\ 10^{-7}$. Our model also provides a good fit to the radial brightness profile of $H^{13}CN$(J=1-0) as shown in Fig. 11. We also investigate the role of line overlap and IR emission on the excitation of the $H^{13}CN$ (J=1-0) transition. The results are shown in Fig. 12. If we consider only the collisions with H_2, the excitation temperatures of F=1-1 and F=0-1 components are comparable. However, when the overlap of hyperfine components is included we find that its effect is to enhance the excitation temperature of the F=1-1 transition while reducing the excitation temperature of the F=0-1 transition. Thus the approximation made by Dayal & Bieging (1995) is qualitatively correct in comparison with the results of our exact calculations. The excitation temperatures of all hyperfine transitions increase substantially when we take into account the absorption of IR photons at 14 μm.

The HCN data are also modelled with the same parameters listed in Table 2. The observed HCN(J=1-0) spectrum at the center position of the envelope is reproduced relatively well with a HCN abundance of $2.5\ 10^{-5}$, giving an isotopic ratio $^{12}C/^{13}C$ = 55 which seems to agree with the results obtained by Nguyen-Q-Rieu et al. (1984), Kahane et al. (1988) and Cernicharo et al. (1991). However, the feature at -43 kms^{-1}, which is due to the F=0-1 component, is much stronger than observed (Fig. 13). This feature shows up in the model spectrum because all three hyperfine components of HCN(J=1-0) transition are found to

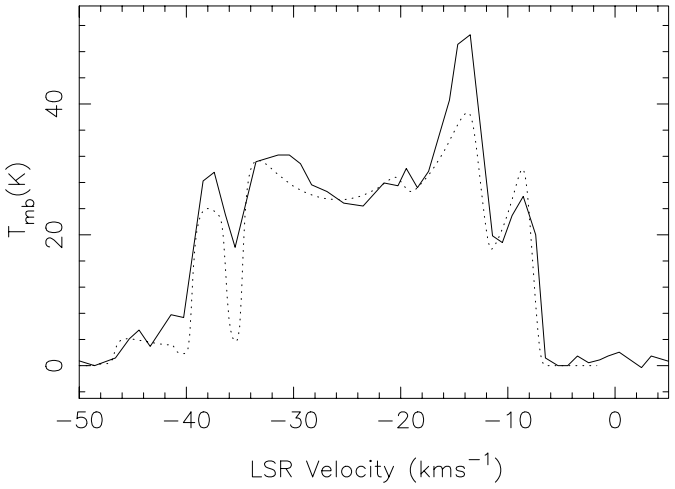

Fig. 10. IRC+10216. Comparison between calculated (dotted line) and observed (solid line) profiles of $H^{13}CN$(J=1-0) taken from Dayal & Bieging (1995) towards the center position of the envelope. The angular resolution is 8 arcsec.

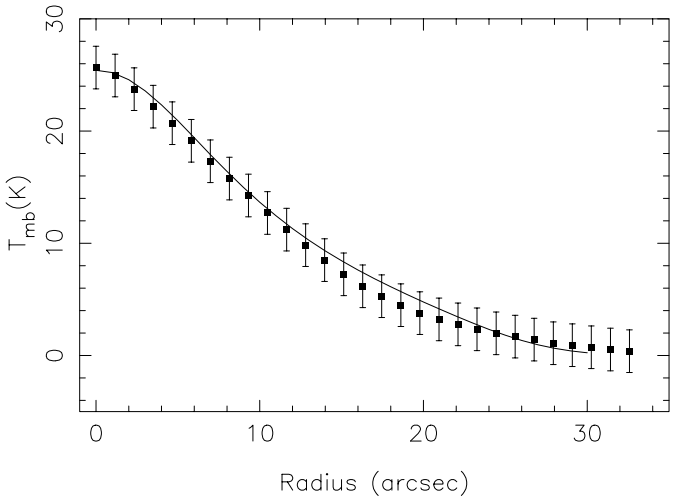

Fig. 11. IRC+10216. The calculated (solid line) and observed radial brightness (squares) profile of $H^{13}CN$(J=1-0) at V_{LSR} = 26.5 kms^{-1} taken from Dayal & Bieging (1995).

be optically thick and to have almost the same excitation temperature. This leads to nearly equal intensity between hyperfine transitions, contrary to the case of $H^{13}CN$. Furthermore, the intensity and the shape of the feature at -37 kms^{-1}, which is due to the F=2-1 component, depend sensitively on the value of the turbulence velocity (V_{turb}) in the envelope. Our model shows that if V_{turb} is too high ($\sim$ 1 kms^{-1}), the intensity and the width of this feature are greatly reduced as the absorption dip at -36 kms^{-1} is enlarged. Thus the value of V_{turb} should be small ($\sim$ 0.5 kms^{-1}). We do not succeed to reproduce the radial brightness profile of the HCN(J=1-0) line (Fig. 14). The sharp decrease of the slope in the observed radial brightness profile of HCN(J=1-0) suggests an abrupt change of excitation conditions of HCN molecule. The likely cause might be an enhancement of the gas density, which corresponds to a higher mass loss rate in the past for IRC+10216. However the $H^{13}CN$(J=1-0) data is satisfactorily fitted with our model using a constant mass loss rate.

5. Discussion

Our non-local radiative transfer model of HCN and $H^{13}CN$ in the circumstellar envelope of carbon stars shows that radiative excitation through the absorption of IR photons (at 3 μm or 14 μm depending on the IR source) plays a dominant role in exciting HCN and $H^{13}CN$ molecules. In optically thin circumstellar envelopes the radiation from the central star with an effective temperature of about 2600–2800 K is not significantly attenuated by the dust. Thus, there are enough IR photons at 3 μm to excite the HCN molecules and to produce the inversion of the ground state HCN(J=1-0) transition. The situation is different in optically thick envelopes. The dust envelope absorbs strongly stellar radiation at short wavelengths and re-emits at longer wavelengths. Thus the role of 3 μm photons is greatly reduced and excitation by 14 μm photons becomes predominant. In all cases investigated in this paper, radiative excitation rates are always comparable or stronger than collisional rates.

From the comparison of our model predictions for Y CVn with observations it seems likely that HCN(J=1-0) line profile contains mostly features of the F=1-1 and F=2-1 components. Early observations carried out by Izumiura et al. (1995a) also show several strong features despite their low spectral resolution. They suggest that the features are F=1-1, F=2-1 and F=0-1 hyperfine components coming presumably from the same clump of gas. The strongest features identified in this way are associated with two clumps separated by about 3 kms^{-1}. That seems to be inconsistent with the expansion velocity, about 8 kms^{-1}, of the gas in the envelope of Y CVn. In addition, the relative intensities of hyperfine components do not agree with our calculations which predict very weak emission from the F=0-1 transition. Since our calculated HCN(J=1-0) line profile matches reasonably the observations we think that the presence of inhomogeneities in the HCN envelope may be able to explain the complex structure of HCN(J=1-0) line profile. The clumpiness of the envelope would be able to produce a profile with more line structure due to the superposition of emission from F=1-1 and F=2-1 hyperfine components. High angular resolution observations will probably help us to see the structure of the envelope very close to the central star.

In our model for the envelope of IRC+10216, rotational transitions in the ($01^{1c}0$) and ($01^{1d}0$) vibrational states are inverted in cascade near the inner radius. The optical depths of the inverted transitions are found to be very small. Observations towards IRC+10216 indicate that only the transition HCN($01^{1c}0$, J=2-1) shows maser emission. This fact suggests that more complicated mechanisms may be involved in the pumping of HCN($01^{1c}0$, J=2-1) maser.

As the rotational levels of HCN are split into hyperfine levels, the overlap between hyperfine transitions is able to redistribute the populations. This phenomenon and its influence is

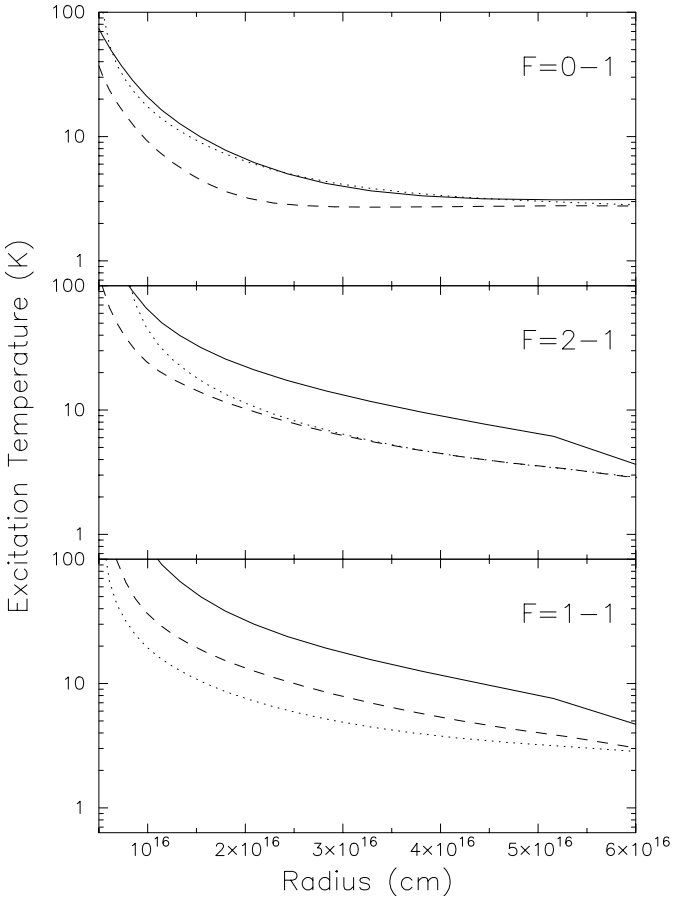

Fig. 12. Excitation temperature of $H^{13}CN$(J=1-0) F=1-1, F=2-1 and F=0-1 hyperfine components in IRC+10216. The dotted line represents the collisional excitation model. The dashed line represents the model when line overlap is included. The solid line represents the model including line overlap, IR excitation and collisions with H_2.

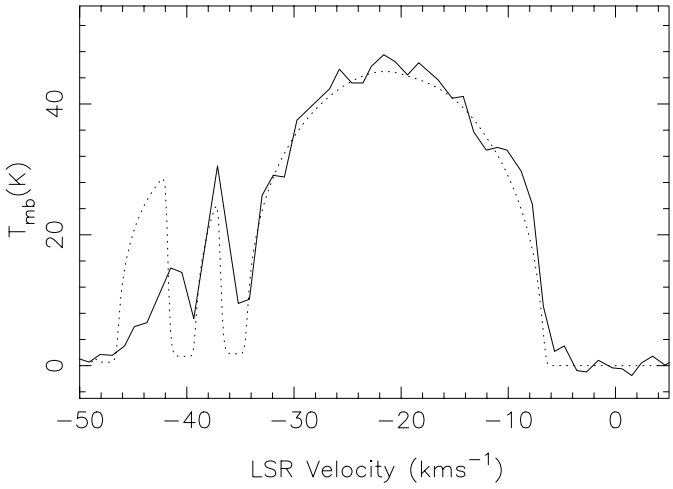

Fig. 13. IRC+10216. Comparison between calculated (dotted line) and observed (solid line) profiles of HCN(J=1-0) taken from Dayal & Bieging (1995) towards the center position of the envelope.

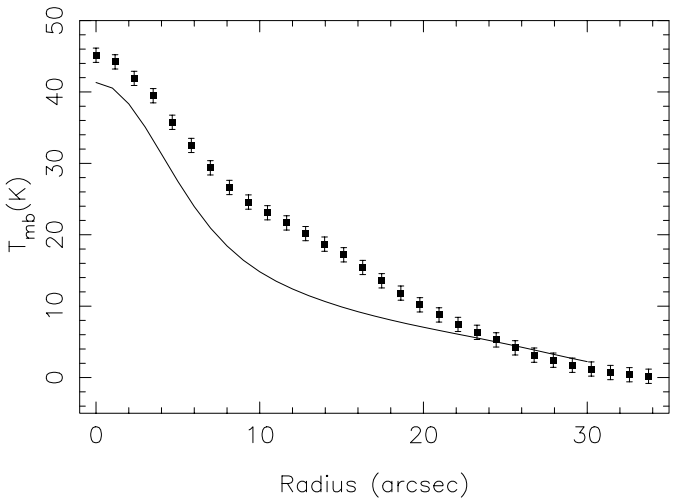

Fig. 14. IRC+10216. The calculated (solid line) and observed (squares) radial brightness profiles of HCN(J=1-0) taken from Dayal & Bieging (1995).

clearly shown in Fig. 12 and can be explained as follows: since the envelope is expanding, at any point in the envelope the emission of the high frequency hyperfine components coming from other parts is red-shifted by the Doppler effect. As a result, the radiation field seen by the lowest frequency component F=1-1 is enhanced by the emissions from the F=2-1 and F=0-1 hyperfine components. Similarly, the intensity of the F=2-1 transition is increased by the emission of the F=0-1 component but the effect is less pronounced. The radiation field enhancement leads to higher excitation temperature of the F=1-1 transition. This phenomenon affects the $H^{13}CN$(J=1-0) line more strongly than the HCN(J=1-0) line since the latter is optically thick and attenuates the radiation of F=2-1 and F=0-1 components coming from other parts of the envelope. The overlap effect is also important to determine the form of the HCN(J=1-0) line profile. As noted before by Truong-Bach & Nguyen-Q-Rieu (1989) the peak of HCN(J=1-0) line profile is shifted toward the red part of the spectrum. Thus HCN(J=1-0) line should not be used to measure the central velocity or the expansion velocity of the circumstellar envelope.

The difficulties encountered when we try to fit the radial brightness profile and the intensity of the feature at -43 kms^{-1} of HCN(J=1-0) line suggest that probably some basic assumptions in our model are not strictly correct for IRC+10216. The most likely is the assumption of a constant mass loss rate. Recent 1.3mm continuum observations of Groenewegen et al. (1997) indicate the presence of dust density enhancement at radii $\sim$ 15 arcsec. Near infrared images of Skinner et al. (1998) show the bipolar morphology of the envelope in the central region. More interestingly, deep V-band images obtained by Mauron & Huggins (1999) reveal a number of concentric rings of dust which are separated by about 5–10 arcsec. That implies a variation of mass loss rate on a timescale of a few hundreds years. However, from the modelling of CO observations Skinner et al. (1999) conclude that there is no evidence for mass loss change in the envelope of IRC+10216. In addition, the $H^{13}CN$ data

studied in this paper do not indicate any enhancement of mass loss rate. We should emphasize here that the evidence against mass loss changes is based on either CO observations which have only limited spatial resolution (usually larger than 12 arcsec) or $H^{13}CN$(J=1-0) line which is optically thin and relatively insensitive to the density of gas. These facts make any effect of mass loss changes difficult to recognize.

6. Conclusion

In this paper we have investigated the excitation of HCN in the circumstellar envelopes of carbon stars. Our results show that the absorption of infrared photons and the overlap of hyperfine transitions are more important than collision with H_2 in exciting HCN molecule. In optically thin envelopes (e.g. Y CVn), radiative pumping through the absorption of $3\,\mu$m stellar photons is capable of creating the inversion of populations in the HCN(J=1-0) transition. The maser amplification and overlap of hyperfine transitions result in a line profile containing several strong spikes. We also show that as the mass loss rate increases above 2 10^{-6} $M_\odot$/yr the inversion in HCN(J=1-0) transition is suppressed. HCN(J=1-0) emission becomes thermal for envelope with higher mass loss rates. In the optically thick envelopes, together with infrared excitation, the overlap between hyperfine transitions also contributes to the excitation of HCN and $H^{13}CN$. Our fit to the interferometric observations of the $H^{13}CN$(J=1-0) line towards IRC+10216 is satisfactory. However, the HCN(J=1-0) data are not totally fitted with our model. High resolution observations of different rotational transitions of CO are therefore necessary to determine the gas density and temperature in the envelope of IRC+10216. Only then we may hope to have a complete understanding of the excitation of HCN molecules.

Acknowledgements. We would like to express our thanks to Dr. T. Le Bertre and Dr. Truong-Bach for fruitful discussions. Our thanks also go to Dr. G. Lefèvre from the GEISA group for providing us the HCN data, Dr. G.R. Knapp for providing us the CO(J=3-2) spectrum of Y CVn and Dr. R. Forster for allowing us to use his HCN(J=1-0) observations of Y CVn.

Appendix A: energy balance model

In the circumstellar envelope the gas temperature is regulated by the heating and cooling processes. The main source of heating is dust-gas collisions. We can express this term as follows:

$$H_{d-g} = \frac{1}{2}\rho_{\rm H_2} v_{\rm drift}^3 n_{\rm d} \pi a_{\rm d}^2 \quad (A.1)$$

$$= \frac{3}{8} m_{\rm H_2}^2 n_{\rm H_2}^2 \frac{\delta}{\rho_{\rm d} a_{\rm d}} \frac{v_{\rm drift}^3}{1 + v_{\rm drift}/v({\rm r})} \quad (A.2)$$

where ρ_d and a_d are dust mass density and the averaged size of dust grain, respectively. δ is the dust to gas ratio and is assumed to be constant throughout the envelope. $v_{\rm drift}$ is the drift velocity of dust grains with respect to the gas component. We use the formula proposed by Kwok (1975) to calculate approximately the drift velocity of the dust grains:

$$v_{\rm drift} = v_{\rm rad}\left[(1+x^2)^{1/2} - x\right]^{1/2} \quad (A.3)$$

where x is calculated in terms of the ratio between the dust velocity due to radiation pressure $v_{\rm rad}$ and the random velocity of the gas $v_{\rm therm}$:

$$x = \frac{1}{2}(v_{\rm therm}/v_{\rm rad})^2 \quad (A.4)$$

and

$$v_{\rm rad} = \left(\frac{L\, v({\rm r})\, Q}{\dot{M} c}\right)^{1/2} \quad (A.5)$$

$$v_{\rm therm} = \frac{3}{4}\left(\frac{3kT_{\rm K}}{m_{\rm H_2}}\right)^{1/2} \quad (A.6)$$

Here L is the stellar luminosity, $v({\rm r})$ is the gas expansion velocity, T_K is the gas kinetic temperature and Q is the dust momentum transfer coefficient.

Another heating mechanism is due to the photoelectric effect. Electrons ejected from dust grains by interstellar UV photons can transfer their excess energy to the gas through collisions. We use here the formula given by Draine (1978):

$$H_{\rm pe} = K_{\rm pe} n_{\rm H_2} \quad (A.7)$$

where the constant K_{pe} is taken to be 2 10^{-26} erg s^{-1}.

The cooling processes are adiabatic expansion and radiative cooling. In our model the contributions to radiative cooling of CO, ^{13}CO, HCN and $H^{13}CN$ molecules are taken into account. Once we know the level populations n_i, it's straightforward to calculate the radiative cooling rate:

$$C = \sum_{k=1}^{n}\left(\sum_{i<k, j\geq k} n_i C_{ij} - n_j C_{ji}\right) h\nu_{kk-1} \quad (A.8)$$

where C_{ij} are the collisional excitation rates. The gas temperature can be determined once we know the heating and cooling terms by solving the energy balance equation:

$$\frac{dT}{dr} = (2-2\gamma)\left(1 + \frac{1}{2}\frac{d\,ln\,v}{d\,ln\,r}\right)\frac{T}{r} + \frac{\gamma-1}{n_{\rm H_2} kv}(H-C) \quad (A.9)$$

Where γ is the adiabatic index, H and C are total heating and cooling rates. We take $\gamma = 5/3$ which is correct for molecular hydrogen at temperature lower than 300 K. We first start with an initial temperature at the inner radius of the envelope and use the LVG approximation to calculate the level populations and thus the cooling rates. Using the above equation we derive the temperature of the next point in the radial direction. The process is repeated again until we reach the outer radius of the envelope.

References

Auer L., 1987, In: Kalkofen W. (ed.) Numerical radiative transfer. Cambridge University Press, p. 101

Auer L., 1991, In: Crivellary L. (ed.) Stellar atmospheres: Beyond classical models. Kluwer, p. 9
Bieging J.H., Chapman B., Welch W.J., 1984, ApJ 285, 656
Cernicharo J., Guélin M., Kahane C., et al., 1991, A&A 246, 213
Cernicharo J., Barlow M.J., Gonzalez-Alfonso E., et al., 1996, A&A 315, L201
Crosas M., Menten K.M., 1997, ApJ 483, 913
Danchi W.C., Bester M., Degiacomi C.G., GreenHill L.G., Townes C.H., 1994, AJ 107, 1469
Dayal A., Bieging J., 1995, ApJ 439, 996
Deguchi S., Nguyen-Q-Rieu, 1990, ApJ 360, L27
De Jong T., Chu Shih-I, Dalgarno A., 1975, ApJ 199, 69
Draine B.T., 1978, ApJS 36, 595
Flower D.R., Launay J.M., 1985, MNRAS 214, 271
Goorvitch D., Chackerian C. Jr., 1994, ApJS 91, 483
Green S., Thaddeus P., 1974, ApJ 191, 653
Groenewegen M.A.T., 1994, A&A 290, 544
Groenewegen M.A.T., 1997, A&A 317, 503
Groenewegen M.A.T., Baas F., de Jong T., Loup C., 1996, A&A 306, 241
Groenewegen M.A.T., van der Veen W.E.C.J., Lefloch B., Omont A., 1997, A&A 322, L21
Guilloteau S., Omont A., Lucas R., 1987, A&A 176, L24
Izumiura H., Ukita N., Kawabe R., et al., 1987, ApJ 323, L81
Izumiura H., Fujiyoshi A., Ukita N., 1995a, Ap&SS 224, 493
Izumiura H., Ukita N., Tsuji T., 1995b, ApJ 440, 728
Justtanont K., Skinner C.J., Tielens A.G.G.M., 1994, ApJ 435, 852
Kahane C., Cernicharo J., Gomez-Gonzalez J., Guélin M., 1988, A&A 190, 167
Knapp G.R., Morris M., 1985, ApJ 292, 640
Knapp G.R., Young K., Lee E., Jorissen A., 1998, ApJ 117, 209
Kwan J., Hill F., 1977, ApJ 215, 781
Kwan J., Linke R.A., 1982, ApJ 254, 587
Kwok S., 1975, ApJ 198, 583
Lambert D.L., Gustafsson B., Eriksson K., Hinkle K.H., 1986, ApJS 62, 373
Lindqvist M., Lucas R., Olofsson H., et al., 1995, Ap&SS 224, 501
Le Bertre T., 1987, A&A 176, 107
Lorenz-Martins S., Lefèvre J., 1994, A&A 291, 831
Lucas R., Cernicharo J., 1989, A&A 218, L20
Lucas R., Guilloteau S., 1992, A&A 259, L23
Lucas R., Guilloteau S., Omont A., 1988, A&A 194, 230
Maki A.G., 1974, J. Phys. Chem. Ref. Data Vol. 3, No. 1, 221
Mauron N., Huggins P.J., 1999, A&A 349, 203
Martin P.G., Rogers C., 1987, ApJ 322, 374
Morris M., 1985, In: Morris M., Zuckerman B. (eds.) Mass loss from red giants. Reidel
Neri R., Kahane C., Lucas R., Bujarrabal V., Loup C., 1998, A&AS 130, 1
Neufeld D.A., Green S., 1994, ApJ 432, 158
Nguyen-Q-Rieu, Bujarrabal V., Olofsson H., Johansson L.E.B., Turner B.E., 1984, ApJ 286, 276
Nguyen-Q-Rieu, Epchtein N., Truong-Bach, Cohen M., 1987, A&A 180, 117
Olofsson H., Eriksson K., Gustafsson B., Carlström, 1993a, ApJS 87, 267
Olofsson H., Eriksson K., Gustafsson B., Carlström, 1993b, ApJS 87, 305
Olofsson H., Lindqvist M., Nyman L.-A., Winnberg A., 1998, A&A 329, 1059
Ridgway S., Keady J.J., 1988, ApJ 326, 843
Rouleau F., Martin P.G., 1991, ApJ 377, 526
Schönberg K., 1988, A&A 195, 198
Skinner C.J., Meixner M., Bobrowsky M., 1998, MNRAS 300, L29
Skinner C.J., Justtanont, Tielens A.G.G.M., et al., 1999, MNRAS 302, 293
Truong-Bach, Nguyen-Q-Rieu, 1989, A&A 214, 267
Truong-Bach, Morris D., Nguyen-Q-Rieu, 1991, A&A 249, 435
Winters J.M., Dominik C., Sedlmayr E., 1994, A&A 288, 255